Journal of Photochemistry and Photobiology A: Chemistry 215 (2010) 1–10

Contents lists available at ScienceDirect

Journal of Photochemistry and Photobiology A: Chemistry

journal homepage: www.elsevier.com/locate/jphotochem

Electrochemical impedance and X-ray photoelectron spectroscopic analysis of dye-sensitized liquid electrolyte based SnO_2/ZnO solar cell

G.R.R.A. Kumara[a,*], Kenji Murakami[b], Masaru Shimomura[b], K. Velauthamurty[a], E.V.A. Premalal[b], R.M.G. Rajapakse[a,b], H.M.N. Bandara[a]

[a] Department of Chemistry, Post-Graduate Institute of Science, University of Peradeniya, Peradeniya, Sri Lanka
[b] Research Institute of Electronics, Shizuoka University, 3-5-1 Johoku, Naka-ku, Hamamatsu 432-8011, Japan

ARTICLE INFO

Article history:
Received 6 November 2009
Received in revised form 8 June 2010
Accepted 15 July 2010
Available online 22 July 2010

Keywords:
Dye-sensitized solar cell
SnO_2/ZnO
Electrochemical impedance spectroscopy
Electron traps

ABSTRACT

A dye-sensitized solar cell based on interconnected SnO_2 nanoparticle matrix covered with a thin outer shell of ZnO, N719 dye, I^-/I_3^- in acetonitrile liquid electrolyte system and lightly platinized FTO counter electrode shows significantly enhanced performance when compared to similar cells made with either pristine SnO_2 or pristine ZnO interconnected nanoparticles. Attempts have been made to investigate the reasons for such an improvement using the information obtained from X-ray photoelectron spectroscopy (XPS) and the electrochemical impedance spectroscopy (EIS). The XPS results reveal that the interconnected nanoparticluar SnO_2 matrix surfaces are fully covered by a ~1 nm thick outer shell of a ZnO layer. EIS results disfavour the idea of direct injection of electrons from the excited dye molecules across the thin outer shell of ZnO into the conduction band of SnO_2 but supports the fact that electrons are first injected to the CB of ZnO and subsequently to the CB of SnO_2 particles both involving trapping and detrapping at each stage. The electron transport along the interconnected SnO_2 nanoparticles also involves anomalous diffusion characterized by a straight line of inclination greater than 45° in the complex impedance plot. This anomalous diffusion is attributed to the trap mediated electron transport.

© 2010 Elsevier B.V. All rights reserved.

1. Introduction

The dye-sensitized nanocrystalline solar cell (DSSC) invented by O'Reagan and Gratzel [1] is a device of tremendous potential for practical applications which has already achieved solar conversion efficiencies as high as 11.5% [2]. The DSSC is composed of an interconnected nanocrystalline TiO_2 particle matrix deposited on a transparent conducting tin oxide glass surface (TCO, commonly used TCO is fluorine-doped tin oxide, FTO) with a typical thickness of less than 15 μm which functions as the active electrode of the solar cell. The commonly used TiO_2 particles known as p-25 are comprised of highly porous spheres of 15–20 nm diameters such that a film of typical thickness of 10 μm to have a roughness factor greater than 1000 which in turn to result in a porosity of 50–70% for sufficient electrolyte film penetration [3]. The interconnected particle surfaces are fully covered with light-absorbing dye molecules [usually Ru(II) dyes with bipyridyl and thiocyanate ligands] which are anchored to TiO_2 surface by means of dative coordination through two carboxylate groups. Lightly platinized TCO plate acts as the counter electrode and the cell is completed by sandwiching a non-aqueous electrolyte (acetonitrile) containing a redox couple (I^-/I_3^- in acetonitrile) between the two electrodes.

While the Gratzel cell is performing so well giving such high energy conversion efficiency, researchers have found that it is not possible if TiO_2 in the DSSC is replaced with other similar oxide semiconductors such as SnO_2 or ZnO [4–7]. The maximum efficiencies recorded are of the order of 1% for the latter systems. However, Tennakone and co-workers have demonstrated that if interconnected SnO_2 nanoparticles are covered with less than 1 nm thin layer of ZnO or interconnected nanoparticles of ZnO are covered with less than 1 nm thin layer of SnO_2, the performance of such DSSCs are dramatically improved compared to those with pristine semiconductor particles [8–10]. Similar results have been obtained when an insulator material is used as the thin outer layer [4,7,11,12]. They have concluded that the main characteristics intrinsic to a semiconductor determining its suitability for DSSCs are the effective electron mass (EEM) and the conduction band position. TiO_2 has a high EEM ($10m_e$ and $50m_e$ according to some reports) and hence is capable of suppressing the recombination of electrons in the TiO_2 matrix with the redox species in the electrolyte (e.g., I_3^-) in contact with it [13]. The EEM values of SnO_2 and ZnO are $0.17m_e$ and $0.19m_e$ respectively and are more than an order of magnitude less than that of TiO_2 [13]. Since the maximum obtainable charge carrier (electrons in this case) mobility is inversely proportional to the effective mass (of

* Corresponding author. Tel.: +94 81 239 4420; fax: +94 81 238 8018.
E-mail address: grakumara2000@yahoo.com (G.R.R.A. Kumara).

1010-6030/$ – see front matter © 2010 Elsevier B.V. All rights reserved.
doi:10.1016/j.jphotochem.2010.07.013

electrons), electrons injected into SnO_2 or ZnO nanocrystalline matrix are expected to have much lower transport time compared to those in the TiO_2. If this is the only reason, given the same number of injected electrons, the DSSCs based on SnO_2 or ZnO should show much superior performance compared to those based on TiO_2. The problem here seems to be that those electrons having much faster mobilities within SnO_2 or ZnO particles can quickly reach their surfaces and perhaps get trapped within available surface states for recombination with the redox species or with the oxidized dye molecules (D^+) in contact with those surface traps. The trapping rate, R_t, and detrapping rate, R_{dt}, are given by $R_t = N_t S(3kT/m^*)^{1/2}$ and $R_{dt} = n_t \omega \exp(-E/kT)$ respectively, where N_t, n_t, S, m^*, E and ω are the density of trapping sites, density of trapped electrons, electron-trap capture cross section, effective electron mass, depth of trapping site below the bottom of the CB and a characteristic frequency of attempting to escape from the trap respectively [8]. The shallow traps are located with $E < kT$ and the trap electrons will, therefore, thermally excite to the CB and thermal excitation and de-excitation are associated with their diffusion along the interconnected nanoparticle matrix. The electrons fallen into deeper traps of $E \gg kT$ will have $R_{dt} \gg R_t$ and their thermal excitation into the CB is, therefore, not possible. These electrons will then undergo recombination with solution species or with the excited dye molecules. We have attempted to determine the energy depths of the trap levels using X-ray absorption spectroscopy (XAS) which could provide information on the unfilled density of states and resonance inelastic X-ray scattering (RIXS) to provide information on the energy depth of filled trap levels. However, this study seems to be difficult and require the development of further fundamental theories to analyze the data and to obtain the energies of trap levels. At present, we are not in a position to calculate the energy depths of trap levels. As explained in Refs. [8–12] a thin outer shell of an insulator or a wide band-gap semiconductor can effectively protect this recombination to result in high conversion efficiencies.

In order to explain the superiority of the SnO_2/ZnO DSC and to account for the effect of thin outer coating of ZnO, Tennakone et al. have proposed the following hypotheses [8].

(i) The excited dye molecules formed due to illumination, inject electrons to the CB of interconnected SnO_2 particles. Since dye molecules are attached to the ZnO outer coating, which is of ~1 nm thickness, the injection of electrons to SnO_2 particles could take place *via* tunnelling through this outer coat and direct tunnelling is very likely as the thickness of ZnO coating is ~1 nm. The ZnO layer then acts only to block the electrons injected into SnO_2 reaching the electrolyte (assuming even and complete surface coverage) so as to suppress recombination of these electrons with the electrolyte species or oxidized dye molecules.

(ii) The excited dye molecules formed due to illumination, inject electrons to the CB of ZnO which subsequently undergo down-hill transition to SnO_2 CB (Fig. 1 shows potentials of the bottoms of CB of ZnO and SnO_2 which clearly show the possibility for the thermodynamically allowed down-hill electron transport). It is quite likely that there are trap levels in both semiconductors and trap mediated transfer is, therefore, very likely. In this situation, the electrons in both SnO_2 and ZnO could undergo recombination with triiodide in solution and the oxidized dye molecules if SnO_2 particles are not fully covered with the ZnO layer.

(iii) The electron injection is same as that in (ii) above but if SnO_2 particles are fully covered by the ZnO layer, the electrons that are injected into SnO_2 particles cannot reach the electrolyte species or oxidized dye molecules for recombination, though the recombination is quite possible for the electrons that exist in the ZnO layer.

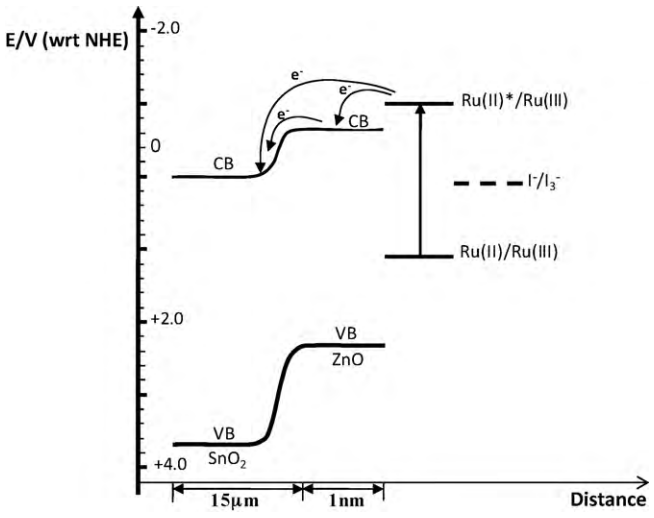

Fig. 1. Schematic energy level diagram showing relative potentials of SnO_2 and ZnO, the ground and excited state redox potentials of the Ru(II)/Ru(III) couple and the I^-/I_3^- redox couple.

Possibilities of electron transfer without involving trapping and detrapping could also be considered but interconnected nanoparticles undoubtedly contain surface traps for electrons and hence such other possibilities could be safely discarded.

In light of these observations and explanations, we have investigated the XPS analysis of SnO_2 particles coated with ZnO outer layer to study the extent of coverage of interconnected SnO_2 particles by the ZnO layer. We have also investigated the EIS behaviour of nanocrystalline SnO_2 particles covered with a thin outer shell of ZnO (SnO_2/ZnO) DSSC. Based on these results we hope to find out the correct mode, out of three possibilities outlined in preceding paragraphs, of electron transfer and transport in the (SnO_2/ZnO) DSSC.

EIS is a powerful electrochemical technique that can be used to study electrical behaviour of metals (corrosion), semiconductors, dielectric materials, electronically conducting inorganic solids and organic polymers, porous materials, ionically conducting materials and many other such systems and also devices based on their combinations and composites. Recently, the EIS analysis of the dye-sensitized nanocrystalline TiO_2 based solar cell (DSC) has attracted a great deal of attention owing to its usefulness in elucidating effective electron transport lifetime along the nanocrystalline TiO_2 matrix, t_t, lifetime of electrons, t_τ, electron transport resistance R_t, interfacial charge recombination resistance, R_{ctTiO_2}, chemical capacitance produced by the accumulation of electrons in the film, C_μ, diffusion lifetime of triiodide ions in the electrolyte, t_{diff}, and many other quantities important for understanding the performance of the device [14–23]. Brisquert has derived theory for the impedance of electron diffusion and recombination in a thin layer configuration such as the DSC and identified four possible cases, *viz*., (i) the impedance of finite diffusion with reflecting boundary, (ii) the impedance of finite diffusion with absorbing boundary, (iii) the impedance of diffusion-reaction in semi-infinite space (Gerischer impedance) and (iv) the impedance that combines Warberg response at high frequency and a reaction arc at low frequency [14]. Brisquert and co-workers have also analyzed the impedance characteristics of the dye-sensitized nanocrystalline TiO_2 based solar cell under various DC bias voltages in the dark as well as under illumination. The effects of both composition and nature of electrolyte, light intensity, semiconductor film thickness etc. on the

performance of the cell have been investigated simply with the help of EIS [15]. They have derived essential theories supported by experimental evidence for analyzing the EIS spectra of many advanced solid state devices including the DSC [16–23]. EIS has been recommended as a useful technique to investigate the long-term stability of the DSSC [24]. Several other reports appear in the literature for the use of EIS in investigating performance of the Gratzel cell and its modified versions [25–28]. In this work we aim at the utilization of the XPS and EIS measurements of SnO_2/ZnO DSSC to investigate the working principle of this solar cell and to understand the reasons for its superiority over DSSCs made of either pristine SnO_2 or pristine ZnO.

2. Materials and methods

2.1. DSC fabrication

Flourine-doped tin oxide (FTO) coated glass plates (1.5 cm × 1.0 cm) were coated with SnO_2/ZnO as described elsewhere [8]. In brief, to a 1.4 cm^3 of colloidal SnO_2 with average particle size 15 nm, 5 drops of glacial acetic acid and 0.04 g of ZnO colloid (average particle size = 3 nm) were added and diluted with 15 cm^3 of ethanol. Mixture was well stirred, 5 drops of Triton-X-100 added and agitated ultrasonically for 10 min. The suspension thus obtained was sprayed on to FTO glass plates heated to 150 °C and sintered in air at 550 °C for 30 min. As in the previous publication, cells with active area 0.25 cm^2 were prepared by covering the FTO plate with a piece of aluminium foil containing a circular aperture of area 0.25 cm^2 and the method also allowed us to control the geometric thickness of the semiconductor layer [8]. The SnO_2/ZnO films thus obtained were coated with the dye, cis-dithiocyanato(N-bis(2, 2′-bipyridyl-4,4′-dicarboxylic acid)) Ru(II), by immersing the hot samples in a warm (∼80 °C) alcoholic solution (3×10^{-3} M) of this dye for 4 h. The films were then removed, rinsed with pure acetonitrile and allowed to dry in air. The cells were then prepared by clamping the plate with the counter electrode (lightly platinized FTO glass) and filling the capillary space with the electrolyte (0.6 M dimethylpropylimidazolium iodide + 0.1 M LiI + 0.05 M I_2 + 0.5 M t-butylpyridine in acetonitrile).

2.2. Electrochemical impedance measurements

Electrochemical impedance spectra were performed for the two DSSCs at selected DC potentials superimposed with a 10 mV AC potential in single sine wave mode using a potentiostat/galvanostat (AUTOLAB PGSTAT 12, ECOCHIMIE) in the frequency range from 0.01 Hz to 10 MHz. The DC potential was applied using a 2-electrode configuration (and not a 3-electrode configuration) and the potential referred to here is the difference in voltages of the FTO electrode baring the dyed semiconductor particles and the lightly platinized FTO counter electrode. Cells were illuminated at 1000 W m^{-2} using a halogen lamp with a UV filter as described in Ref. [8]. To avoid heating effects a water jacket was placed between the cell and the light source.

2.3. X-ray photoelectron spectroscopic measurements

In order to determine the surface coverage of interconnected SnO_2 particles by ZnO particles and to estimate the thickness of the ZnO layer, X-ray photoelectron spectroscopic (XPS) studies were performed for samples preheated at 100 °C for 20 min to remove any adsorbed moisture. XPS measurements were performed using ESCA-LAB Mk II (VG) with an Al/Mg twin anode X-ray source. Al K_α and Mg K_α lines, respectively, were used to determine the film thickness and the Auger parameter analysis.

3. Results and discussion

3.1. Summary of previous results

As revealed in the previous publication, the morphology of the SnO_2/ZnO semiconductor particle matrix is such that large (∼15 nm) interconnected SnO_2 particles are expected to be coated with ∼0.8 nm thin layer of ZnO and this DSSC has produced I_{sc} of 16.9 mA cm^{-2}, V_{oc} of 665 mV, a fill factor of 0.65 giving an overall efficiency of 7.3% under 1.5 AM 1000 W m^{-2} illumination [8]. However, the DSSC made of interconnected SnO_2 without ZnO coating layer gave much lower values (I_{sc} of 12.5 mA, V_{oc} of 330 mV, a fill factor of 0.31 giving an overall efficiency of 1.3% under the same conditions) [8]. The SEM or TEM pictures presented there, however, did not provide conclusive evidence to the presence of ZnO outer shell particularly when the expected thickness is of 1 nm order. EDX showed the distribution of Sn and Zn but experimental evidence to the presence of ZnO on the surface of SnO_2 was provided only by the dye desorption experiments [8]. In the method of preparation, SnO_2 colloidal particles (15 nm) are mixed with sufficient amount of ZnO and 15% excess of acetic acid is added to dissolve all ZnO particles. The spraying solution, therefore, has SnO_2 particles and Zn^{2+} ions with acetate as the anion. Of course, when the thin layer sprayed onto FTO glass plate is dried Zn^{2+} ions are expected to be adsorbed onto the SnO_2 particles. The firing at 550 °C would burn away the organic species present in the system and under ordinary atmospheric conditions it is quite possible to form ZnO on the SnO_2 particles.

3.2. X-ray photoelectron spectroscopic analysis

XPS offers precise thickness measurements for ultra thin films. Fig. 2a shows survey spectrum for the surface of ZnO covered SnO_2 particles. The spectrum mainly consists of Zn, Sn, and O peaks. In the spectrum, no contamination related peaks are detected except for the very weak C 1s and Cl 2p peaks, which may only have negligibly small effect to the electronic properties of the material. Thickness of the film can be estimated by using Eq. (1) given below [29].

$$t = \lambda \cos\theta \ln\left(1 + \frac{I_o/S_o}{I_s/S_s}\right) \quad (1)$$

The parameters in Eq. (1) are: t the thickness of the film, λ is the attenuation length of the photoelectrons in the film, θ is the emission angle which has been set to 0 in this experiment, I_o and I_s are the measured peak intensities from the over-layer (Zn $2p_{3/2}$) and the substrate (Sn $3d_{3/2}$) respectively, and S_o and S_s are their sensitivity factors [30]. The attenuation length, λ, is calculated by averaging the inelastic mean free paths (IMFPs) of ZnO and SnO_2 using TPP-2 M formula [31]. From Eq. (1), the thickness of the ZnO film calculated using these experimental results is 1.2 ± 0.2 nm. Since the ZnO film is coated on the spherical SnO_2 particles, the real thickness would be thinner than the calculated value of 1.2 nm as the calculation makes the assumption of a flat film. This estimated thickness of ZnO film is in good agreement with that reported previously [8].

Fig. 2b shows the Zn $2p_{3/2}$ peak of the SnO_2/ZnO film. The spectrum can be fitted by single component of Voigt function. Though the chemical environment is considered to be uniform for the whole surface, the binding energy of 1021.7 eV is applicable not only to Zn in its oxide but also for metallic Zn. To distinguish between metallic Zn and Zn^{2+} in its oxide, Auger parameter analysis using the Mg K_α excitation source was performed. The kinetic energy of Zn LMM Auger line obtained at 988.6 eV is in good agreement with Zn^{2+} in ZnO [32]. Thus, it can be concluded that the surface of the film is covered with a continuous film of ZnO layer with homoge-

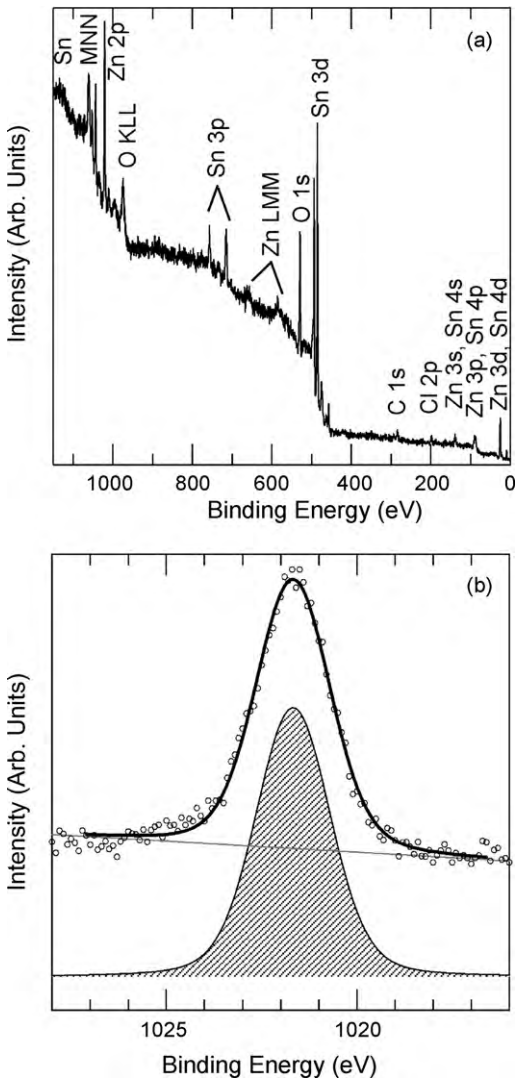

Fig. 2. (a) XPS survey spectrum for the surface of the ZnO/SnO_2 film. (b) Zn $2p_{3/2}$ XPS peak of the ZnO/SnO_2 film together with curve fitting results. The peak position is at 1021.7 eV.

neous thickness of 1.2 ± 0.2 nm. This analysis is very useful because the complete surface coverage will eliminate possibilities for the recombination of electrons in SnO_2 particles with the triiodide ions in the electrolyte as the ZnO layer now acts as a barrier between the SnO_2 particles and the electrolyte.

3.3. Electrochemical impedance spectroscopic analysis

3.3.1. EIS data of SnO_2/ZnO DSC in the dark

The analysis becomes straightforward when we consider the EIS spectra recorded in the dark at different DC voltage bias values. When the DC potential (all Dc potentials referred in here are with reference to the counter electrode) is well below the bottom of CB of SnO_2 particles, the electrons supplied to FTO cannot be injected into SnO_2 CB and hence interconnected semiconductor matrix should behave as an insulator. As the potential is increased in the negative direction, a situation is reached at which the applied potential is close to the potential of the bottom of CB of SnO_2 particles, the Fermi Level of SnO_2 is raised towards the CB and the material then becomes conducting. Since the spectra are recorded in the dark and electrons are injected from the FTO, complications do not arise from the dye injecting electrons and recombination with oxidized dye cations. The Nyquist plots recorded in the dark are depicted in Fig. 3 and their corresponding Bode plots are shown in the Supplementary Fig. S1.

First of all, we see that these EI spectra given in Fig. 3a–d resemble, to a certain extent, to those reported by Fabregat-Santiago et al. for the TiO_2 DSC, and hence a suitable comparison is possible between the two systems [15]. Another striking possibility is the ability to adopt at least a modified version of the theory derived by the same group on the EIS of dye-sensitized nanocrystalline semiconductor solar cells under different DC applied potentials. Although the Nyquist plots at different applied potentials look different at quick glance (Sets with similar appearance are grouped together in Fig. 3a–d) careful investigation shows that even at low applied potentials (Curve set in Fig. 3a) the plots have a small semicircle at highest frequencies and another large semicircle at low-frequency domain (Also a small straight line part inclined at an angle greater than 45° after the first semicircle can be distinguished). The two semicircular arches could be attributed to the serial connection of the parallel combination of R_{FTO} and C_{FTO} elements and the parallel combination of R_{Pt} and C_{Pt} elements. The initial *x*-axis intercept tells us about the resistance of the FTO surface and the straight line describes the transport resistance associated with the diffusion of electrons along the interconnected SnO_2 particle matrix (which is very large at low applied potentials in the dark).

When the applied potential is close to the potential of the bottom of the CB of SnO_2, the straight line with gradient greater than 1 (angle of inclination greater than 45°) becomes clearly visible and another semicircle also appears at even lower frequencies as in Fig. 3b (features of just one curve in the curve set of Fig. 3b are enlarged in the inset). Presumably the frequency range allowed in the instrument would be sufficient to record the fourth feature when the system is conducting but the low-frequency regime is insufficient to locate the fourth feature when the applied potential is more positive than the potential of the bottom o the CB (in the potential vertical axis the applied potential is well below the potential of the bottom of the CB of SnO_2) so that the semiconductors are behaving as insulators. At potentials more negative than the potential of the bottom of the CB of SnO_2, only three semicircular arches are observed.

3.3.2. Processes and equivalent circuits

Let us, therefore, begin by figuring out a schematic diagram of key components of the SnO_2/ZnO solar cell (Fig. 4a) and a suitable equivalent circuit diagram to describe the processes associated with it (Fig. 4b and c). We notice here that some modifications to the circuit elements proposed for the Grätzel cell may be required to assemble an equivalent circuit for the present system. First of all, we see that there is a resistance, R_{FTO}, associated with the electron transport through the FTO surface. There is an uncovered part of FTO which is in contact with the redox species present in the electrolyte as the electrolyte penetrates to the FTO surface *via* pores of the semiconductor matrix (other sides of these pores are exposed to the ZnO coating since SnO_2 particles are fully covered by ZnO) and hence electrons in the FTO surface can recombine with the solution species. In terms of electrical elements, there is a charge-transfer resistance R_{FTO} in parallel combination with the capacitance of the triple junction FTO/semiconductor/electrolyte, C_{FTO}. The electrons injected into the SnO_2 particles are transported along the interconnected SnO_2 particle matrix leading to electrical elements of r_t (=R_t per unit length L) which are in series connection to create a rail of so called transmission line. Diffusion of solution species creates a semi-infinite Warberg impedance, $Z_{d(sol)}$ and the charge transfer at the Pt/electrolyte interface creates a parallel combination of charge-transfer resistance, R_{Pt}, and an interfacial capacitance, C_{Pt}, at this interface. The three circuit elements, *viz.*, the parallel combination of R_{FTO} and C_{TCO}, the $Z_{d(sol)}$ and the parallel combination of

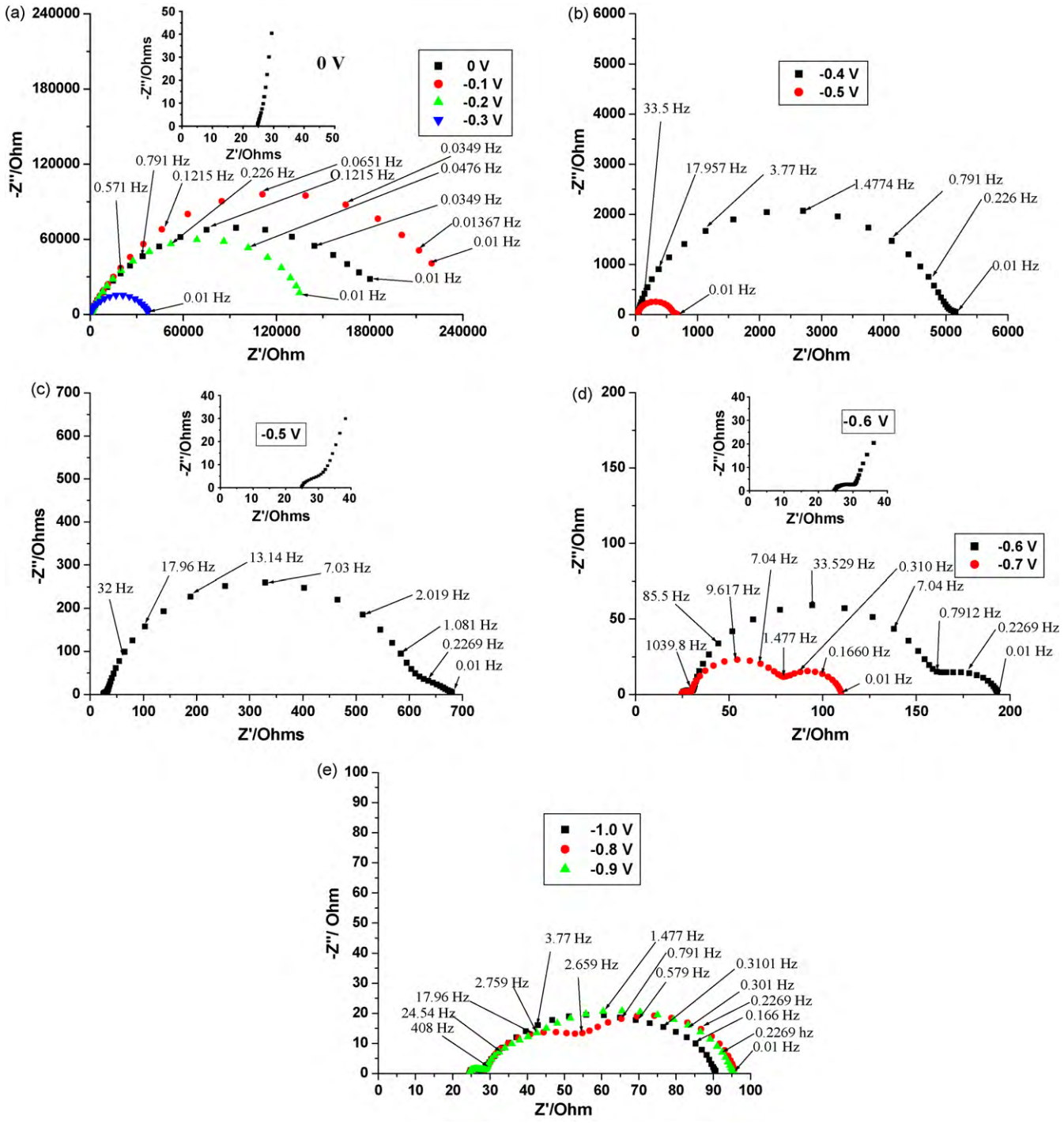

Fig. 3. The Nyquist plots for the EI spectra of SnO_2/ZnO DDSC in the dark at selected DC bias voltages. Insets are shown for some selected plots.

R_{Pt} and C_{Pt} in serial connection form the second rail of the dual rail transmission line. Contrary to the situation of the Grätzel cell, the SnO_2 particles are not in contact with the electrolyte solution provided that all the exposed surfaces of interconnected particles are covered with the ZnO layer. If this is the case, then only the outer surface of the outer ZnO thin layer is exposed to the electrolyte. If we assume that the photogenerated electrons tunnel straight into the SnO_2 particles crossing the ZnO boundary and their reversal into ZnO is not possible, then there will be no recombination with the solution species (or with the oxidized dye molecules) until their passage to the FTO surface. For this situation, however, we have to consider another capacitance term called the chemical capacitance, C_μ. The origin of which has been clearly explained by Brisquert et al. [18] in an excellent review on electrochemical determination of the density of states of nanostructured metal-oxide semiconductors. When a voltage variation dV is applied to the conductive substrate holding the nanostructured semiconductor film, the Fermi level of the semiconductor is homogeneously displaced by an amount of dE_{Fn} which is given by $dE_{Fn} = -q\,dV$, where q is the elementary charge, and as a consequence the electron density changes by an amount of dn. The electrochemical capacitance (per unit volume, volume capacitance density) created as a result of these changes is

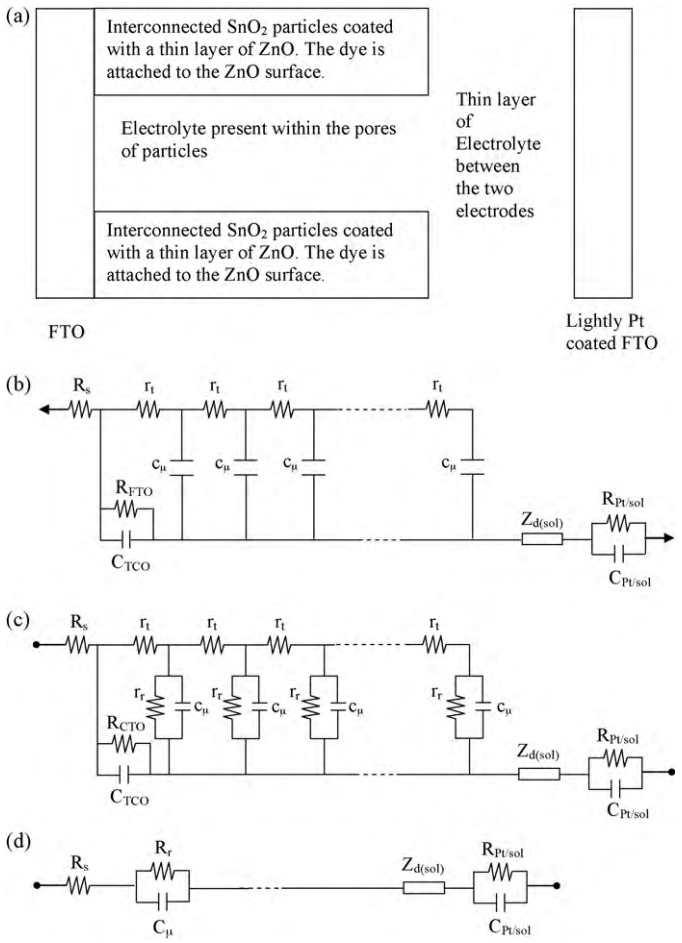

Fig. 4. (a) A schematic representation of the components of the SnO_2/ZnO DSSC. (b) The proposed equivalent circuit for the whole cell if the electrons injected from the dye tunnels straight into the SnO_2 particles and proceed to the FTO plate without recombination during their path. (c) The proposed equivalent circuit for the whole cell if the electrons injected from the dye are first injected to ZnO CB and subsequently transfer to SnO_2 particles *via* trap mediated transport. (d) Simplified equivalent circuit applicable to the situation close to V_{oc}.

given by

$$C_\mu = q\frac{dn}{dF_{Fn}} \quad (2)$$

Since SnO_2 particles are expected to be unexposed to the electrolyte, the generation of Helmholtz capacitance or charge-transfer capacitance is unlikely. However, the chemical capacitance generated by the change of chemical potential of electrons in SnO_2 particles due to change in the number of electrons as a result of potential perturbation is to be considered. There is also a possibility for trap mediated diffusion of charge carriers within the interconnected SnO_2 particles as documented earlier for TiO_2 [33,34] and ZnO [35,36]. The electrons in the traps are in thermal equilibrium with those in the conduction band (CB) and the change in potential by dV can introduce a trap capacitance C_T in addition to the CB capacitance C_{CB} but the two capacitances (C_T and C_{CB}) are additive [16] as they are connected in parallel to each other and the sum may be taken as C_μ. These capacitances will be in parallel connection between each of r_t elements as depicted in the circuit diagram in Fig. 4b. Since the SnO_2 particles are not exposed to the electrolyte or the oxidized dye cations the recombination of trap electrons in it with the solution species or oxidized dye cations is not possible and hence the assumption that trap electrons are in thermal equilibrium with CB electrons is justifiable.

For such an equivalent circuit given in Fig. 4b, at low negative applied potentials in the dark, when the semiconductor matrix is acting as an insulator and the Warberg impedance due to diffusion of solution species also negligible, a semicircle displaced from the origin by a value of R_s (=R_{FTO}) can be expected if the parallel RC circuit due to the Pt/electrolyte interface is also neglected. The appearance of the small semicircle in the low-frequency region in Fig. 3b could be assigned to the serial connection of the equivalent circuit due to Pt/electrolyte interface. The large semicircle depicts the parallel connection of R_{FTO} and C_{FTO} and the analysis of the EIS spectra at potentials much lower than the potential of the bottom of the CB of SnO_2 would then give the magnitudes of these quantities (Supplementary Table S1 gives related resistance and capacitance data together with relevant frequency ranges and time constants).

When the applied potential is sufficiently negative and close to the potential of the CB of SnO_2 particles, the equivalent circuit depicted in Fig. 4b would reduce to a simpler version as the resistance of the semiconductor matrix is negligible under these circumstances. The equivalent circuit will then be a serial connection of four components: R_s, C_μ, $Z_{d(sol)}$ and the parallel combination of R_{Pt} and C_{Pt} (see Fig. 4d). Under these circumstances, one cannot expect to see three semicircles since there is no resistance in parallel to C_μ, one would expect only a totally capacitive vertical line in place of a semicircle.

However, Fig. 3c clearly shows the presence of three semicircles together with an additional line inclined at an angle greater than 45° in the Nyquist plots recorded in the dark at potentials close to the potential of the bottom of CB of SnO_2. The Bode plots depicted in Supplementary Fig. S1 under these conditions also show three characteristic frequencies corresponding to three characteristic local maxima. These results, therefore, rule out the simplest equivalent circuit diagram proposed for the system and provide the implication for the necessity of having electron transfer at the SnO_2/electrolyte or ZnO/electrolyte interface or both, i.e., the necessity for the involvement of the recombination of electrons with solution species.

3.3.3. *Case for exposed SnO_2 particles*

If the SnO_2 particle surfaces are not fully covered with ZnO thin film, the electrolyte could then penetrate into those uncovered areas. The possibility then exists for recombination of some of the electrons, particularly those that are trapped in surface states for a sufficiently lengthy time, with the triiodide ions in the solution in contact with such uncovered surfaces. This then creates parallel RC circuit elements to describe the charge-transfer resistance associated with the recombination of electrons at the SnO_2/electrolyte interface, R_r (=R_r/L) and the chemical capacitance due to the change of electron density as a function of the Fermi level. The overall result is none other than the transmission line model proposed for the EIS characteristics of the Grätzel cell. Indeed the EIS characteristics shown in Fig. 3 and those given for the Grätzel cell are similar in shapes at comparable potentials, i.e., lower range, middle range and around the potential at the bottom of the CB of SnO_2. However, XPS studies revealed that the SnO_2 particle surfaces are fully covered with the ZnO layer. This indicates tat the electrons injected to the CB of SnO_2 cannot undergo recombination with solution species or with oxidized dye molecules at the SnO_2 surface.

3.3.4. *Recombination at the ZnO surface*

These arguments then bring us to the suggestion that the possibility of direct tunnelling of electrons into the CB of SnO_2 across the thin layer of ZnO is very unlikely. We, therefore, propose that the RC circuit elements required forming the parallel connections between the rails of transmission lines should come from the ZnO surface exposed to the electrolyte. This means that the excited dye molecules should first inject electrons to the conduction band of the

ZnO layer. Those electrons then have two possible paths, *viz.*, (i) to fall into surface traps within the band gap of ZnO and (ii) to relax into the CB of SnO_2 particles in contact with ZnO particles again *via* down-hill process. Arguably, both these processes could take place and are required to explain the observed EIS characteristics of the system. Those that are fallen into shallow traps of ZnO could thermally re-excite into the CB and follow both paths (i) and (ii) and those electrons in trap levels and the CB of a semiconductor can be assumed to be in thermal equilibrium and those that are lived long enough to recombine with the solution species would do so. Based on these processes the theoretical analysis of the observed trends the EI spectra of SnO_2/ZnO cell in the dark at selected DC potentials applied wrt the counter electrode and under illumination are now given below.

The impedance spectra of the SnO_2/ZnO cell around with applied potentials close to the potential of the bottom of the CB of SnO_2 also consists of four characteristic features: the leftmost horizontal straight line along the *x*-axis (the displacement) that can be attributed to the serial connection of the Ohmic resistance of the FTO surface (R_s), the leftmost semicircle arc ($\omega_{max} = \omega_1$) corresponding to the charge transfer at the Pt/electrolyte interface (the charge-transfer resistance $R_{Pt/electrolyte}$ in parallel combination with the capacitance at the Pt/electrolyte interface $C_{Pt/electrolyte}$), a straight line inclined at an angle greater than 45° corresponding to the diffusion of electrons along the interconnected semiconductor particle network (at around frequency ω_2, which is a small feature hidden inside the large semicircle, see insets in Fig. 3), middle semicircular arc ($\omega_{max} = \omega_3$) corresponding to the charge transfer at the ZnO/solution interface by recombination and finally a third semicircular arc at lowest frequencies corresponding to the diffusion of triiodide ions in the electrolyte ($\omega_{max} = \omega_4$). The last term is generally referred to as the Nernst impedance, Z_N which is given by the following formula.

$$Z_N = \frac{W}{\sqrt{i\omega}} \tanh\left(\sqrt{\frac{i\omega}{K_N}}\right) \quad (3)$$

where W is the Warberg parameter defined by $W = kT/n_2 q c_{I_3^-} A\sqrt{D_{I_3^-}}$ and $K_N = D_{I_3^-}/\delta^2$.

The symbols have their usual meanings, k the Boltzmann constant, T absolute temperature, A electrode area, c concentration, D diffusion coefficient, n number of electrons transferred per reaction event and q the elementary charge. This under absorbing boundary condition gives rise to a deformed semicircle at low frequency [14].

When the applied potential (wrt the counter electrode) is close to the potential of the bottom of the CB of SnO_2, i.e., when the Fermi Level is raised close to the bottom of the CB, the interconnected semiconductor particle matrix behaves as a full conductor and we notice that ω_2 always appearing at a value higher than ω_3 at each applied potential (Supplementary Table S1). This means that the transport time, t_t, is always lower than the lifetime, t_τ, due to the recombination of electrons with the solution species before reaching the FTO surface. This is a clear indication of the proper functioning of the solar cell as the electrons are now able to reach the FTO surface before most of them being removed by the recombination with the solution species. Thus the shielding of SnO_2 particles by a thin layer of ZnO particles helps prevent the recombination of electrons injected into SnO_2 particles.

3.3.5. Comparison with the EIS results of the Grätzel cell

Of interest here is to compare the characteristic frequencies (or time constants) for the present system with those already published for the Grätzel cell by (AQ) Hoshikawa et al. [27]. When the same composition of the electrolyte [0.6 M dimethylpropylimidazolium iodide + 0.1 M LiI + 0.05 M I_2 + 0.5 M t-butylpyridine in acetonitrile] is used for the Grätzel cell they have reported that $\omega_1 = 15$ kHz, $\omega_3 = 40$ Hz and $\omega_4 = 0.6$ Hz at the V_{oc}. The corresponding values for the present system as depicted in Table S1 are $\omega_1 = 17$ kHz, $\omega_2 = (45–218)$ Hz, $\omega_3 = 9.6$ Hz and $\omega_4 = 0.42$ Hz at around V_{oc}. We see clearly that both ω_1 and ω_4 are almost comparable in the two systems but ω_3 differs significantly such that ω_3 is 4 times lower in SnO_2/ZnO system in comparison to that of TiO_2 system. This means that the recombination of electrons at the TiO_2/electrolyte interface is 4 times slower than that at the SnO_2/ZnO/elctrolyte system. Although the effective electron masses of ZnO or SnO_2 are an order of magnitude lower than that of TiO_2 so that electrons in ZnO or SnO_2 could travel 10 times faster than those in TiO_2, the electrons in SnO_2 or ZnO undergo 4 times faster recombination with electrolyte species compared to those in TiO_2. Implication brought about here is that there are much deeper traps in both ZnO and SnO_2 compared to those in TiO_2 so that electron transport in the former systems is governed mainly by the trap mediated diffusion along interconnected particles.

3.3.6. Straight line portion of the impedance spectra

Another important feature that is noticeable in the impedance spectra of the SnO_2/ZnO system when compared to that of TiO_2 system is the difference in the gradient of the straight line appearing between the first and second semi-circular arches. These gradients are much higher than 1 at each potential studied and hence the angle of inclination is much greater than 45° (see Table S1). As revealed by Fabregat-Santiago et al. [15] under the condition of $R_t < R_r$ (or $\omega_k < \omega_d$), the equation for the diffusion-reaction model (Eq. (4))

$$Z = \left(\frac{R_t R_r}{1 + i\omega/\omega_k}\right)^{1/2} \coth\left[\left(\frac{\omega_k}{\omega_d}\right)^{1/2}\left(1 + i\frac{\omega}{\omega_k}\right)^{1/2}\right] \quad (4)$$

where $\omega_d = D_n/L^2 = 1/R_t C_\mu$ is the characteristic frequency of diffusion in a finite layer, D_n is the chemical diffusion coefficient of electrons, L is the path length of diffusion, $\omega_k = 1/R_r C_\mu$ is the characteristic frequency (rate constant) of recombination and ω is the angular frequency, reduces to the conventional Warberg impedance described by Eq. (5) giving rise to a straight line of slope 1.

$$Z = R_t\left(i\frac{\omega}{\omega_d}\right)^{1/2} \quad (5)$$

For the TiO_2 based system they obtained this feature between the first and second semicircular arches (as a small feature hidden between the semicircles but clearly shown in insets). The gradient of the straight line they observed was 1. However, for the present system, the similar feature is almost hidden in between the first and second semicircular arches (shown clearly in insets) though the gradient is not exactly 1 and we find that it is always greater than 1 at each DC bias (Supplementary Table S1). This suggests that the ordinary diffusion of electrons along the interconnected TiO_2 particles assumed for the Grätzel cell is not strictly applicable to the SnO_2/ZnO cell. As expected, there can be trap levels within the SnO_2 particles and the electrons in the CB and the trap levels are in thermal equilibrium. Transport of electrons along the interconnected SnO_2 particles is essentially dependent upon the rates of electron trapping and detrapping. This means that the electron diffusion is not an ordinary diffusion but a kind of anomalous one as observed for impedance of porous electrodes in which transport is governed by the drift in the electrical field [37]. Brisquert and Compte [21] have also derived theory for the electrochemical impedance of anomalous diffusion by modifying the normal Warberg impedance by introducing a factor β ($0 < \beta < 2$) such that $Z(i\omega) \propto (i\omega)^{-\beta/2}$. They then obtained relationships for a system with anomalous diffusion under usual conditions of reflecting boundary and absorbing

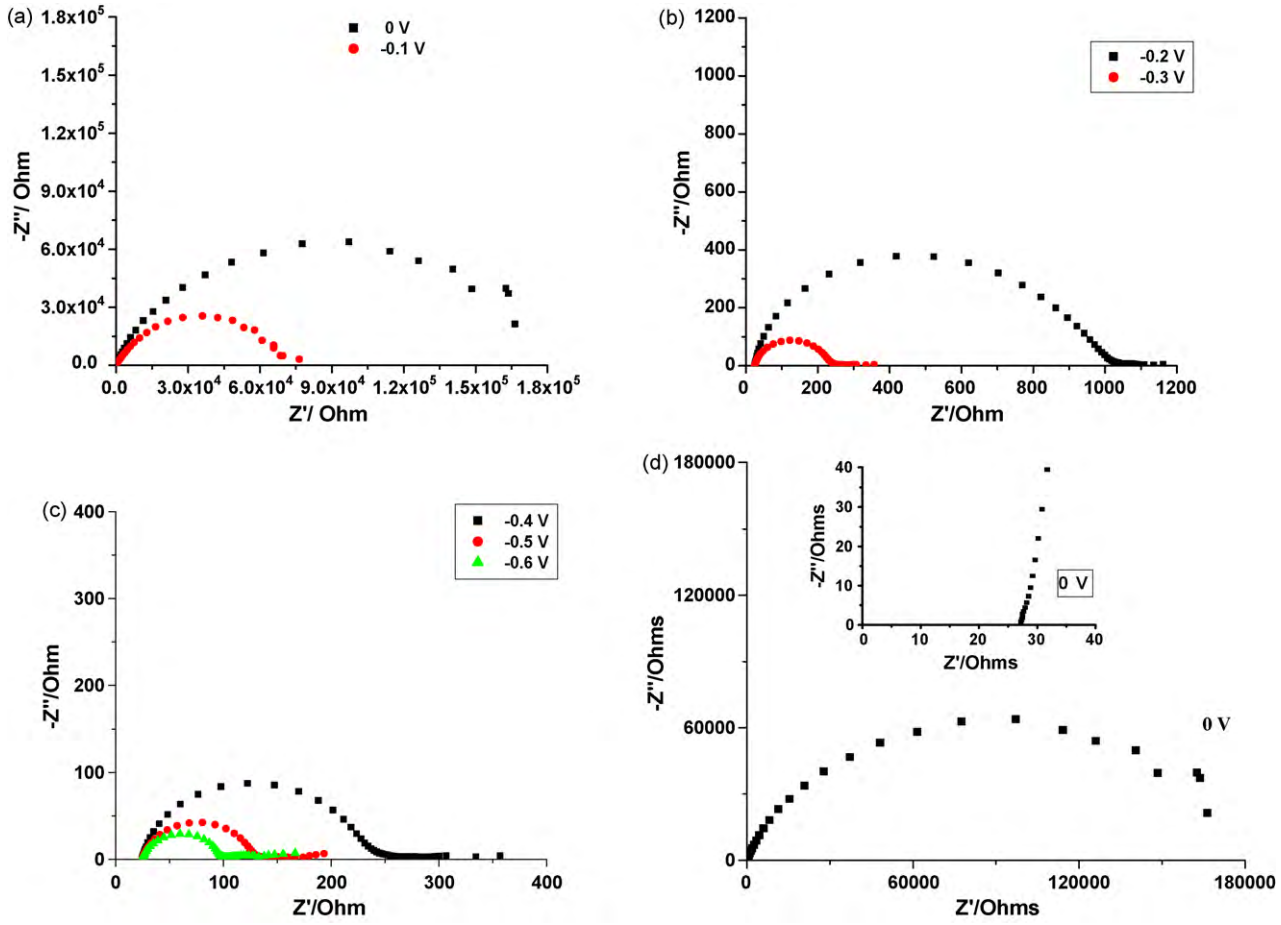

Fig. 5. The Nyquist plots for SnO_2/ZnO DSSC at different DC potentials under illumination.

boundary. For the reflecting boundary the impedance is given by

$$Z(s) = R_W \left(\frac{\omega_d}{s}\right)^{\gamma/2} \coth\left[\left(\frac{s}{\omega_d}\right)\right]^{\gamma/2} \quad (6)$$

where $\gamma < 1$.

This function reduces to

$$Z(s) = R_W \left(\frac{\omega_d}{s}\right)^{\gamma/2} \quad (7)$$

at high frequency and is a straight line in the Nyquist plot inclined at an angle less than 45°.

On the other hand, for the absorbing boundary condition, the impedance is given by

$$Z(s) = R_W \left(\frac{\omega_d}{s}\right)^{\gamma/2} \tanh\left[\left(\frac{s}{\omega_d}\right)\right]^{\gamma/2} \quad (8)$$

and this also yields the above same expression at high frequency giving rise to a straight line inclined at an angle of less than 45°. Clearly this type of anomalous diffusion is to be ruled out for our system.

The second type of anomalous diffusion they have described requires the following functions to explain the observed behaviour. For this type of anomalous diffusion with reflecting boundary condition gives rise to the impedance function

$$Z(s) = R_W \omega_d^{1-\gamma} \left(\frac{\omega_d}{s}\right)^{\gamma/2} \coth\left(\frac{s}{\omega_d}\right)^{\gamma/2} \quad (9)$$

The limiting behaviour of this function at high frequency is

$$Z(s) = R_W \omega_d^{\gamma-1} \left(\frac{\omega_d}{s}\right)^{1-\gamma/2} \quad (10)$$

which for $\gamma < 1$ gives rise to a straight line inclined at an angle greater than 45°.

For the absorbing boundary condition, the impedance function is given by,

$$Z(s) = R_W \omega_d^{1-\gamma} \left(\frac{\omega_d}{s}\right)^{\gamma/2} \tanh\left(\frac{s}{\omega_d}\right)^{\gamma/2} \quad (11)$$

which again gives rise to the same reduced form at high frequency with a straight line inclined at an angle greater than 45°.

Our results clearly agree with this type of anomalous diffusion and whether the electrons reached at the FTO surface are reflected back or absorbed, the Nyquist plot yields a straight line inclined at an angle greater than 45°.

The reason for the observed anomalous diffusion is most likely due to the trap mediated diffusion. The electrons in the CB of the semiconductor particles are in thermal equilibrium with those fallen into the trap levels. Hence the trapping and detrapping of electrons are essential steps in their diffusion towards the FTO surface. Since SnO_2 particles are covered with ZnO particles and hence their recombination with solution species is suppressed the slow transport would not create a problem of losing the efficiency of the cell. This may also explain why SnO_2 or ZnO based DSCs are much inferior to the TiO_2 based DSC.

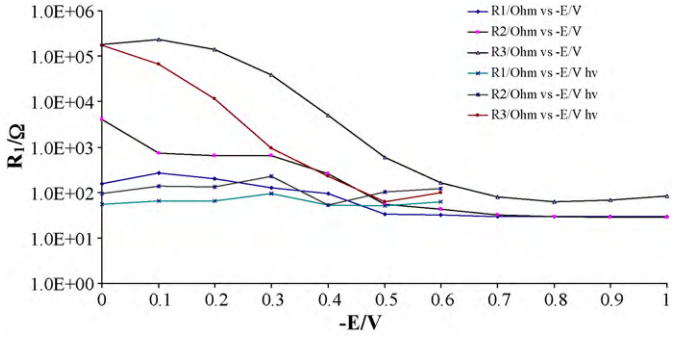

Fig. 6. The variation R_1, R_2 and R_3 values calculated from the Nyquist plots as a function of DC potential applied in the dark as well as under illumination.

3.3.7. EIS data under illumination

Having analyzed the EIS of the SnO_2/ZnO DSC at different DC voltages in the dark, let us now consider the same under illumination. Fig. 5 depicts the Nyquist plots for the EIS of the same under illumination and the data extracted are given in Supplementary Table S2. The variation of R_1, R_2 and R_3 values in the dark at different DC voltages as well as under illumination (labeled $h\nu$) are shown in Fig. 6. It is clear from these graphs the corresponding resistance values are three to two orders of magnitude lower from their dark values when the cell is illuminated. This is an expected result as even without electron supply from the FTO the cell will function as the light absorbed by the dye injects electrons to the semiconductor matrix and all subsequent processes will take place. Another important factor to be noticed is that under illumination there are no significant changes in the resistance values with increasing negative DC bias.

4. Conclusions

The performance of SnO_2 based DSC can be dramatically improved if the recombination of electrons can be suppressed. This could be achieved conveniently by covering the outer surfaces of interconnected SnO_2 particles by a thin outer shell of a ZnO layer. The XPS investigation of the SnO_2/ZnO DSC thus formed confirms the complete and uniform surface coverage of SnO_2 particles by ZnO and estimates the thickness of the ZnO layer to be ~1 nm. The photo-excited dye molecules inject electrons first into the CB of the ZnO and subsequently to the CB of SnO_2 both involving trapping and detrapping processes. The electron transport along the interconnected SnO_2 also involves anomalous diffusion characterized by trapping and detrapping which is clearly indicated by the straight line of gradient greater than 1 in the complex impedance plots. Since the SnO_2 particles are covered the electrons in the SnO_2 particles do not undergo recombination during their passage towards the FTO electrode resulting in improved performance of the solar cell. Electrons injected to ~1 nm thick ZnO outer layer are efficiently transferred to the CB of interconnected SnO_2 but the recombination of electrons in the ZnO layer with solution species and/or oxidized dye molecules is possible.

Acknowledgement

We acknowledge the financial support of the National Research Council of Sri Lanka Equipment Grant NRC 05-07.

Appendix A. Supplementary data

Supplementary data associated with this article can be found, in the online version, at doi:10.1016/j.jphotochem.2010.07.013.

References

[1] B. O'Reagan, M. Gràtzel, Nature 353 (1991) 737–740.
[2] C.Y. Chen, M. Wang, J.Y. Li, N. Pootrakulchote, L. Alibabaei, C.H. Ngoc-le, J.D. Decoppet, J.H. Tsai, C. Gratzel, C.G. Wu, S.M. Zakeeruddin, M. Gratzel, ACS Nano 3 (2009) 3103–3109.
[3] J.M. Kroon, N.J. Bakker, H.J.P. Smit, P. Liska, K.R. Thampi, P. Wang, S.M. Zakeeruddin, M. Gra¨tzel, A. Hinsch, S. Hore, U. Wu¨rfel, R. Sastrawan, J.R. Durrant, E. Palomares, H. Pettersson, T. Gruszecki, J. Walter, K. Skupien, G.E. Tulloch, Prog. Photovolt.: Res. Appl. 15 (2007) 1–18.
[4] K. Tennakone, I.R.M. Kottegoda, L.A.A. De Silva, V.P.S. Perera, The possibility of ballistic electron transport in dye-sensitized semiconductor nanocrystalline particle aggregates, Semicond. Sci. Technol. 14 (1999) 975–978.
[5] K. Tennakone, G.R.R.A. Kumara, I.R.M. Kottegoda, V.P.S. Perera, An efficient dye-sensitized photoelectrochemical solar cell made from oxides of tin and zinc, J. Chem. Soc. Chem. Commun. (1999) 15–16.
[6] K. Tennakone, J. Bandara, K.M.P. Bandaranayake, G.R.R. Kumara, A. Konno, Enhanced efficiency of a dye-sensitized solar cell made from MgO-coated nanocrystalline SnO_2, J. Appl. Phys. 40 (2001) L732–L734.
[7] G.R.R. Kumara, K. Tennakone, V.P.S. Perera, A. Konno, S. Kaneko, M. Okuya, Suppression of recombinations in a dye-sensitized photoelectrochemical cell made from a film of tin IV oxide crystallites coated with a thin layer of aluminium oxide, J. Phys. D: Appl. Phys. 34 (2001) 868–873.
[8] G.R.R. Kumara, K. Tennakone, I.R.M. Kottegoda, K.M.P. Bandaranayake, A. Konno, M. Okuya, S. Kaneko, K. Murakami, Efficient dye-sensitized photoelectrochemical cells made from nanocrystalline tin(IV) oxide-zinc oxide composite films, Semicond. Sci. Technol. 18 (2003) 312–318.
[9] K. Tennakone, K.M.P. Bandaranayake, P.V.V. Jayaweera, A. Konno, G.R.R. Kumara, Dye-sensitized composite semiconductor nanostructures, Physica E 14 (2002) 190–196.
[10] M. Gratzel, International Workshop on Nanostructures in Photovoltaic, 28 July–4 August, Dresden, Germany, 2001.
[11] M.K.I. Senevirathna, P.K.D.D.P. Pitigala, E.V.A. Premalal, K. Tennakone, G.R.A. Kumara, A. Konno, Stability of the SnO_2/MgO dye-sensitized photoelectrochemical solar cell, Sol. Energy Mater. Sol. Cells 91 (2007) 544–547.
[12] Z. Liu, K. Pan, M. Liu, M. Wang, Q. Lü, J. Li, Y. Bai, T. Li, Al_2O_3-coated SnO_2/TiO_2 composite electrode for the dye-sensitized solar cell, Electrochim. Acta 50 (2005) 2583–2589.
[13] N. Tsuda, K. Nasu, A.K. Fujikori, Siratori in Electronic Conduction in Oxides, 2nd ed., Springer, 2002, ISSN0171-1873.
[14] J. Brisquert, Theory of the impedance of electron diffusion and recombination in a thin layer, J. Phys. Chem. B106 (2002) 325–333.
[15] F. Fabregat-Santiago, J. Brisquert, G. Garcia-Belmonte, G. Boschollo, A. Hagfeldt, Influence of electrolyte in transport and recombination in dye-sensitized solar cells studied by impedance spectroscopy, Sol. Energy Mater. Sol. Cells 87 (2005) 117–131.
[16] J. Brisquert, Influence of the boundaries in the impedance of porous film electrodes, Phys. Chem. Chem. Phys. 2 (2000) 4185–4192.
[17] J. Brisquert, F. Fabregat-Santiago, I. Mora-Seró, G. Garcia-Belmonte, E.M. Barea, E. Palomares, A review of recent results on electrochemical determination of the density of electronic states of nanostructured metal-oxide semiconductors and inorganic hole conductors, Inorg. Chim. Acta 361 (2008) 684–698.
[18] J. Brisquert, Physical electrochemistry of nanostructured devices, Phys. Chem. Chem. Phys. 10 (2008) 49–72.
[19] J. Gracia-Cañadas, F. Fabregat-Santiago, H.J. Bolink, E. Palomares, G. Garcia-Belmonte, J. Brisquert, Determination of electron and hole energy levels in mesoporous solid state dye solar cell, Synth. Met. 156 (2006) 944–948.
[20] I. Mora-Seró, J.A. anta, T. Dittrich, G. Garcia-Belmonte, J. Brisquert, Continuous time random walk simulation of short-range electron transport in TiO_2 layers compared with transient surface photovoltage measurements, J. Photochem. Photobiol. A: Chem. 182 (2006) 280–287.
[21] J. Brisquert, A. Compte, Theory of electrochemical impedance of anomalous diffusion, J. Electroanal. Chem. 499 (2001) 112–120.
[22] J. Brisquert, G. Garcia-Belmonte, F. Fabregat-Santiago, P.R. Bueno, Theoretical models for ac impedance of diffusion layers exhibiting low frequency dispersion, J. Electroanal. Chem. 475 (1999) 152–163.
[23] J. Brisquert, A. Zaban, The trap-limited diffusivity of electrons in nanoporous semiconductor networks permeated with a conductive phase, Appl. Phys. A 77 (2003) 507–514.
[24] R. Kern, R. Sastravan, J. Ferber, R. Stangl, J. Luther, Modeling and interpretation of electrical impedance spectra of dye solar cells operated under open-circuit conditions, Electrochim. Acta 47 (2002) 4213–4225.
[25] T. Hoshhikawa, T. Ikebe, R. Kikuchi, K. Eguchi, Effect of electrolyte in dye-sensitized solar cells and evaluation by impedance spectroscopy, Electrochim. Acta 51 (2006) 5286–5294.
[26] Seok-Soon Kim, Jun-Ho Yum, Yung-Eun Sung, Improved performance of a dye-sensitized solar cells using a TiO_2/ZnO/Eosin Y electrode, Sol. Energy Mater. Sol. Cells 79 (2003) 495–505.
[27] G. Kron, T. Egerter, G. Nelles, A. Yasuda, J.H. Werner, U. Rau, Electrical characterization of dye sensitized nanocrystalline TiO_2 solar cells with liquid electrolyte and solid-state organic hole conductor, Thin Film Solids 403 (2002) 242–246.
[28] K.-M. Lee, V. Suryanarayanan, K.-C. Ho, A study on the electron transport properties of TiO_2 electrodes in dye-sensitized solar cells, Sol. Energy Mater. Sol. Cells 91 (2007) 1416–1420.

[29] J.M. Hill, D.G. Royce, C.S. Fadley, L.F. Wagner, F.J. Grunthaner, Properties of oxidized silicon as determined by angular-dependent X-ray photoelectron spectroscopy, Chem. Phys. Lett. 44 (1976) 225–231.
[30] C.D. Wagner, L.E. Davis, M.V. Zeller, J.A. Taylor, R.H. Raymond, L.H. Gale, Empirical atomic sensitivity factors for quantitative analysis by electron spectroscopy for chemical analysis, Surf. Interface Anal. 3 (1981) 211–225.
[31] S. Tanuma, C.J. Powell, D.R. Penn, Calculations of electron inelastic mean free paths. V. Data for 14 organic compounds over the 50–2000 eV range, Surf. Interface Anal. 21 (1994) 165–176.
[32] G. Schoen, Auger and direct electron spectra in X-ray photoelectron studies of zinc, zinc oxide, gallium and gallium oxide, J. Electron Spectrosc. Relat. Phenom. 2 (1973) 75–86.
[33] R. Könenkamp, Carrier transport in nanoporous TiO_2 films, Phys. Rev. B 61 (2000) 11057–11064.
[34] T. Dittrich, E.A. Lebedev, J. Weidmann, Erratum to electron drift mobility in porous TiO_2 (Anatase), Phys. Status Solidi A 167 (1998) R9.
[35] J. Brisquert, A. Zaban, P. Salvador, Analysis of the mechanisms of electron recombination in nanoporous TiO_2 dye-sensitized solar cells. Nonequilibrium steady-state statistics and interfacial electron transfer via surface states, J. Phys. Chem. B 106 (2002) 8774–8782.
[36] E.A. Meulenkamp, Electron transport in nanoparticulate ZnO films, J. Phys. Chem. B 103 (1999) 7831–7838.
[37] J. Brisquert, G. Garcia-Belmonte, F. Fabregat-Santiago, N.S. Ferriols, P. Bogdanoof, E.C. Pereira, Doubling exponent models for the analysis of porous film electrodes by impedance. Relaxation of TiO_2 nanoporous in aqueous solution, J. Phys. Chem. B 104 (2000) 2287–2298.